AGU PUBLICATIONS

JGR

Journal of Geophysical Research: Space Physics

BRIEF REPORT

10.1002/2014JA020919

Key Points:
- A wave number 2 QTDW is identified in the MLT region
- This W2 possibly results from the nonlinear interaction between W3 and SPW
- The observations agree well with numerical simulations

Correspondence to:
S.-Y. Gu,
shengyanggu@gmail.com

Citation:
Gu, S.-Y., H.-L. Liu, T. Li, X. Dou, Q. Wu, and J. M. Russell III (2015), Evidence of nonlinear interaction between quasi 2 day wave and quasi-stationary wave, *J. Geophys. Res. Space Physics*, *120*, 1256–1263, doi:10.1002/2014JA020919.

Received 4 DEC 2014
Accepted 15 JAN 2015
Accepted article online 2 FEB 2015
Published online 25 FEB 2015

Evidence of nonlinear interaction between quasi 2 day wave and quasi-stationary wave

Sheng-Yang Gu[1,2,3], Han-Li Liu[3], Tao Li[1,2], Xiankang Dou[1,2], Qian Wu[3], and James M. Russell III[4]

[1]CAS Key Laboratory of Geospace Environment, Department of Geophysics and Planetary Science, University of Science and Technology of China, Hefei, China, [2]Mengcheng National Geophysical Observatory, School of Earth and Space Sciences, University of Science and Technology of China, Hefei, China, [3]High Altitude Observatory, National Center for Atmospheric Research, Boulder, Colorado, USA, [4]Center for Atmospheric Sciences, Hampton University, Hampton, Virginia, USA

Abstract The nonlinear interaction between the westward quasi 2 day wave (QTDW) with zonal wave number $s = 3$ (W3) and stationary planetary wave with $s = 1$ (SPW1) is first investigated using both Thermosphere, Ionosphere, and Mesosphere Electric Dynamics (TIMED) satellite observations and the thermosphere-ionosphere-mesosphere electrodynamics general circulation model (TIME-GCM) simulations. A QTDW with westward $s = 2$ (W2) is identified in the mesosphere and lower thermosphere (MLT) region in TIMED/Sounding of the Atmosphere using Broadband Emission Radiometry (SABER) temperature and TIMED/TIMED Doppler Imager (TIDI) wind observations during 2011/2012 austral summer period, which coincides with a strong SPW1 episode at high latitude of the northern winter hemisphere. The temperature perturbation of W2 QTDW reaches a maximum amplitude of ~8 K at ~30°S and ~88 km in the Southern Hemisphere, with a smaller amplitude in the Northern Hemisphere at similar latitude and minimum amplitude at the equator. The maximum meridional wind amplitude of the W2 QTDW is observed to be ~40 m/s at 95 km in the equatorial region. The TIME-GCM is utilized to simulate the nonlinear interactions between W3 QTDW and SPW1 by specifying both W3 QTDW and SPW1 perturbations at the lower model boundary. The model results show a clear W2 QTDW signature in the MLT region, which agrees well with the TIMED/SABER temperature and TIMED/TIDI horizontal wind observations. We conclude that the W2 QTDW during the 2011/2012 austral summer period results from the nonlinear interaction between W3 QTDW and SPW1.

1. Introduction

The westward quasi 2 day wave (QTDW) with zonal wave number 3 (W3) is a predominant phenomenon at the mesosphere and lower thermosphere (MLT) region of the austral summer hemisphere shortly after the solstice [*Wu et al.*, 1996; *Gu et al.*, 2013]. The W3 QTDW is proposed to be the Rossby-gravity (3, 0) mode [*Salby*, 1981], which could be influenced by the barotropic/baroclinic instabilities related with the background zonal wind [*Plumb*, 1983; *Limpasuvan et al.*, 2000; *Salby and Callaghan*, 2001; *Liu et al.*, 2004; *Yue et al.*, 2012].

Compared with W3 QTDW, only a few studies report QTDW with westward zonal wave number 2 (W2) and its origin. *Riggin et al.* [2004] reported a W2 QTDW with horizontal wind observations from the High Resolution Doppler Imager instrument on board the UARS. The meridional wind perturbations were observed to maximize in the equatorial region at the mesopause. This W2 QTDW was suggested to be excited in situ at upper mesospheric heights, which has little direct connection with the 2 day activity at lower altitude. *Limpasuvan and Wu* [2009] found anomalous 2 day wave activities with W2 in the mesospheric temperature and line-of-sight wind from the Microwave Limb Sounder (MLS) instrument on board the Aura satellite, which was suggested to be an unstable mode induced by atmosphere instabilities. A W2 unstable mode with a period of 49 h was also found by *Rojas and Norton* [2007] in a linear two-dimensional instability model simulation under the boreal summer easterly condition. Its global structure showed a maximum amplitude at middle- and high-latitude regions in the summer hemisphere for both temperature and neutral wind. Moreover, the zonal wind perturbations also exhibited a smaller peak at low latitude in the winter hemisphere, and the meridional wind perturbations had a smaller peak at the equator. The Aura/MLS temperature data sets showed active W2 QTDW oscillations during January with maximum amplitude at middle and low latitudes and minimum amplitude at the equator [*Tunbridge et al.*, 2011].

The nonlinear interaction between planetary-scale waves can contribute to atmosphere variability. For example, the nonlinear interaction between W3 QTDW and the migrating diurnal tide has been studied by

Palo et al. [2007], which generates an eastward $s = 2$ QTDW. The thermosphere-ionosphere-mesosphere electrodynamics general circulation model (TIME-GCM) simulation showed that although the quasi-stationary planetary wave is incapable of propagating directly into the ionosphere or to low latitudes due to the critical layers and strong molecular dissipation, the planetary wave and tidal interaction can induce large changes in tides and then transmit planetary wave signals into the ionosphere at low and middle latitudes [*Liu et al*., 2010]. *Pancheva et al*. [2002, 2004] reported the nonlinear interactions between the W3 QTDW and the 16 day planetary wave with wave number 1, while the nonlinear interactions between QTDW and stationary planetary waves have not been reported yet.

In this paper, the nonlinear interactions between W3 QTDW and stationary planetary wave with $s = 1$ (SPW1) are investigated with both satellite observations and TIME-GCM simulations. The data set and numerical experiment are presented in section 2. Shown in section 3 are the analysis results from both observations and simulations, followed by a summary in section 4.

2. Data Set and Methodology

2.1. TIMED Observations

The TIMED Doppler Imager (TIDI) and the Sounding of the Atmosphere using Broadband Emission Radiometry (SABER) instruments on board the Thermosphere, Ionosphere, and Mesosphere Electric Dynamics (TIMED) satellite measure the mesospheric horizontal wind and temperature, respectively. The National Center for Atmospheric Research (NCAR)-processed TIDI data provide neutral winds between 85 and 105 km with a vertical resolution of 2.5 km [*Killeen et al*., 2006]. SABER is a limb-viewing infrared radiometer that measures the temperature profiles from ~20 to ~120 km [*Mertens et al*., 2004]. A least squares fitting method is applied to both the version 0307A TIDI and version 1.07 SABER observations from December 2011 to February 2012, to extract the amplitudes of the QTDW within a temporal window of 6 days. Latitudinal windows of 10° and 20° are utilized for SABER and TIDI observations, respectively, due to the much sparser sampling points of TIDI.

2.2. TIME-GCM Simulations

The National Center for Atmosphere Research TIME-GCM is a time-dependent and self-consistent three-dimensional model from the upper stratosphere to the thermosphere [*Roble and Ridley*, 1994]. The version of TIME-GCM used in this study simulates global neutral atmosphere and the ionospheric dynamo electric field at a $5° \times 5°$ horizontal resolution and 0.5 scale height vertical resolution. The gravity wave parameterization based on linear saturation theory by *Lindzen* [1981] is utilized in the model. Both migrating diurnal and semidiurnal tides from the global-scale wave model are forced at the lower model boundary.

Since the lower boundary of TIME-GCM is ~30 km and the dynamics below 30 km are not resolved, a westward propagating wave number 3, 2 day wave with geopotential height perturbations of 1000 m is forced at the lower boundary. The Gaussian-shaped geopotential height perturbations for W3 QTDW peak at 30°N, extending from 10°S to 70°N. A zonal wave number 1 stationary planetary wave with geopotential height perturbations of 1500 m is also forced at the lower boundary. The Gaussian-shaped geopotential height perturbations for SPW1 peak at 60°N, extending from 35°N to 85°N. The model perpetually runs for 40 days with the calendar date set to 20 January, and each day is numbered days 1–40. Both the forcing of W3 QTDW and SPW1 are fully added on day 10 with a Gaussian-shaped increasing tendency from days 1 to 10. The forcing of W3 QTDW is attenuated with a Gaussian-shaped decreasing tendency from days 25 to 40. The forcing of SPW1 is sustained from days 10 to 40.

3. Results

Figure 1a shows the least squares fitted spectrum of SABER temperature observations at 88 km and 25°S during 1–6 January 2012. The dominant wave propagates westward with zonal wave number 2 and period of ~2 days. Figure 1b shows the least squares fitted spectrum of SABER temperature observations at 84 km and 25°S during 20–25 January 2012, which shows a westward propagating planetary wave with zonal wave number 3 and period of ~2 days. The wave number-period spectra of the TIDI wind observations show similar QTDW signals as the SABER temperature observations (not shown). Thus, both the wave number 2 and wave number 3 QTDW signatures are identified in the MLT region in January 2012.

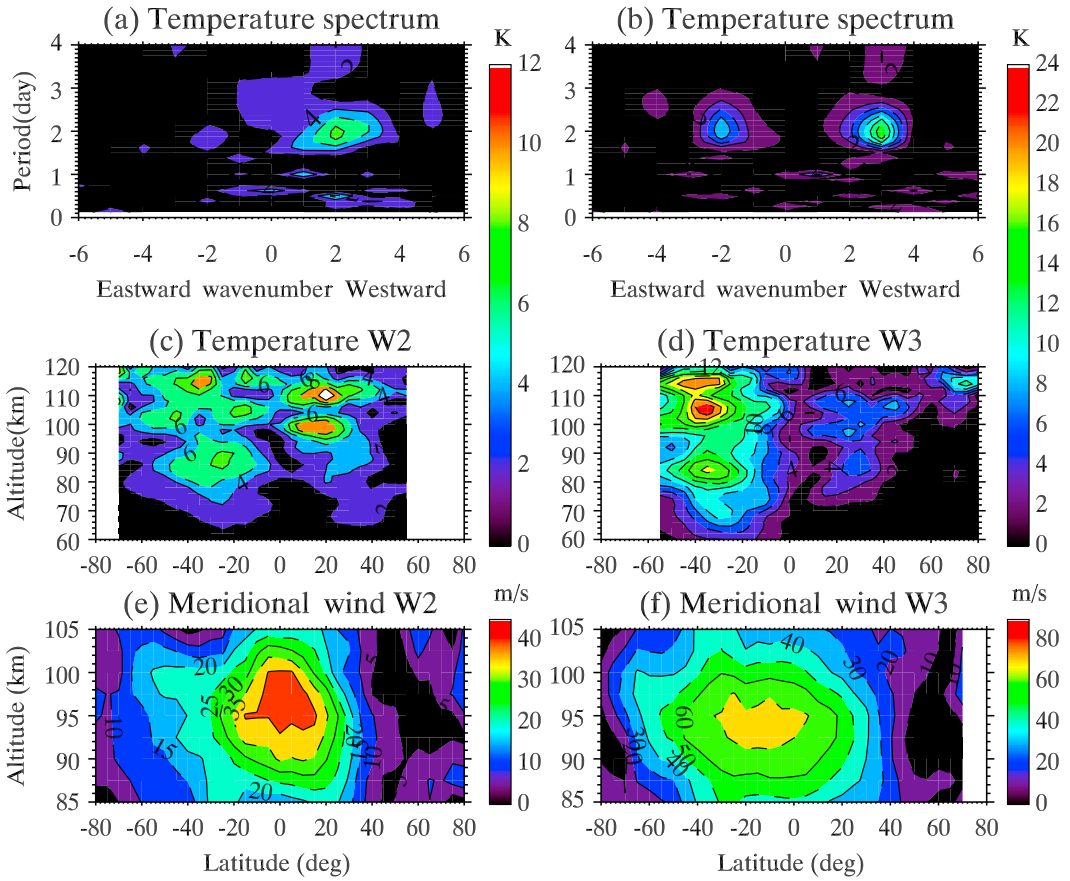

Figure 1. The least squares fitting spectrum for SABER temperature observations (a) at 88 km and 25°S during 1–6 January 2012 and (b) at 84 km and 30°S during 20–25 January 2012. The vertical and latitudinal distributions of the (c, e) W2 and (d, f) W3 QTDW in SABER temperature (Figures 1c and 1d) and TIDI meridional wind (Figures 1e and 1f) are also shown.

Shown in Figure 1c is the vertical-latitude structure from the W2 QTDW in SABER temperature during 1–6 January 2012. The SABER temperature samplings cover from ~80°S to ~50°N during this period. In the Southern Hemisphere, the W2 QTDW in temperature maximizes at ~30°S with amplitude of ~8 K and ~10 K at ~88 km and ~115 km, respectively. The perturbations of the temperature W2 QTDW in the Southern Hemisphere increase from 60 km to ~88 km and reach a minimum at ~95 km. In the Northern Hemisphere, the W2 QTDW in temperature peaks at ~20°N with maximum amplitudes of ~10 K and ~12 K at ~100 km and ~110 k, respectively. The perturbations of W2 QTDW in temperature reach minimum amplitude at the equator. Figure 1e shows the cross section of the W2 QTDW in meridional wind obtained from TIDI observations during 1–6 January 2012. The TIDI wind covers 80°S–80°N with both cold and warm side observations. The W2 QTDW meridional wind perturbations maximize in the equatorial regions between 95 km and 100 km, with maximum amplitude of ~40 m/s. Figures 1d and 1f show the vertical-latitude structures of W3 QTDW in temperature and meridional wind, respectively. The temperature perturbations of W3 QTDW are much stronger in the Southern (summer) Hemisphere than in the Northern (winter) Hemisphere. The summer hemisphere perturbations peak at ~30°S with amplitudes of ~16 K and ~26 K at ~84 km and ~108 km, respectively. The winter hemisphere perturbations maximize at ~30°N with amplitudes of only ~6 K and ~8 K at the similar altitudes. The maximum meridional wind perturbations of W3 QTDW of ~65 m/s are located at ~95 km at low latitudes in the Southern Hemisphere. It is stronger than the maximum amplitude of W2 QTDW. In all, both the W2 and W3 QTDW events in SABER temperature and TIDI wind observations agree well with the previous studies [*Limpasuvan and Wu*, 2009; *Tunbridge et al.*, 2011; *Gu et al.*, 2013].

Figure 2a shows the temporal variation of the W2 QTDW amplitude in SABER temperature at 88 km, where it reaches maximum amplitude in the Southern Hemisphere, as shown in Figure 1c. The W2 QTDW grows

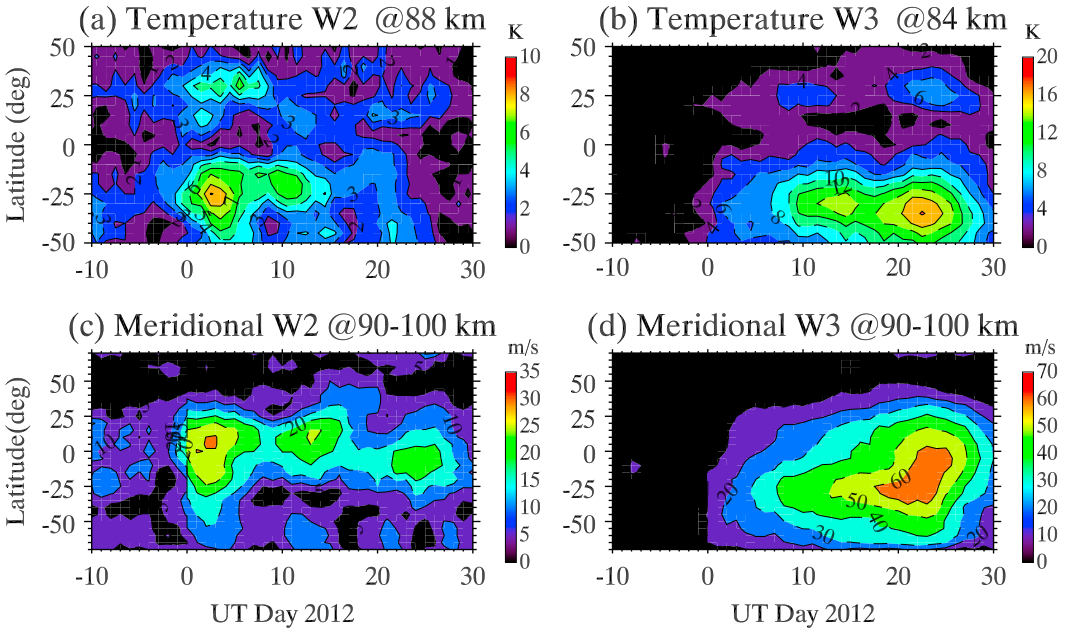

Figure 2. The temporal and latitudinal variations of the (a, c) W2 and (b, d) W3 QTDW. The W2 and W3 QTDW in temperature (Figures 2a and 2b) are obtained with SABER observations at 88 km and 84 km, respectively. The W2 and W3 QTDW in meridional wind are obtained with TIDI observations between 90 and 100 km.

gradually from the end of December 2011, with a peak on around 3 January 2012. At this altitude, the perturbations reach larger amplitudes in the Southern Hemisphere than in the Northern Hemisphere. The maximum amplitude is ~8 K at ~25°S and only ~5 K at ~25°N. Between days 10 and 12, the W2 QTDW reaches a secondary peak with maximum amplitude of ~6 K at ~25°S. Figure 2c shows the temporal variation of the W2 QTDW amplitude in meridional wind between 90 and 100 km, which agrees well with the temporal variation in SABER temperature. The meridional wind perturbations also maximize at the beginning of January 2012 with a maximum amplitude of ~30 m/s at the equator. In addition, a secondary peak of ~25 m/s is observed at around day 12.

Figures 2b and 2d show the temporal variations of the W3 QTDW amplitude in SABER temperature at 84 km and TIDI meridional wind between 90 and 100 km, respectively. It is clear that the temperature perturbations of W3 QTDW are also weaker in the Northern Hemisphere than in the Southern Hemisphere. In the Northern Hemisphere, the W3 QTDW shows two peaks around 14 and 23 January with amplitudes of ~4 K and ~6 K, respectively. In the Southern Hemisphere, the amplitudes of W3 QTDW on around days 14 and 23 are ~14 K and ~16 K. The meridional wind perturbations of W3 QTDW peak at around day 23 with maximum amplitude of ~60 m/s at low latitudes in the Southern Hemisphere. At the beginning of January 2012, the W3 QTDW amplitudes are ~6–8 K and ~20–30 m/s for temperature and meridional wind, respectively.

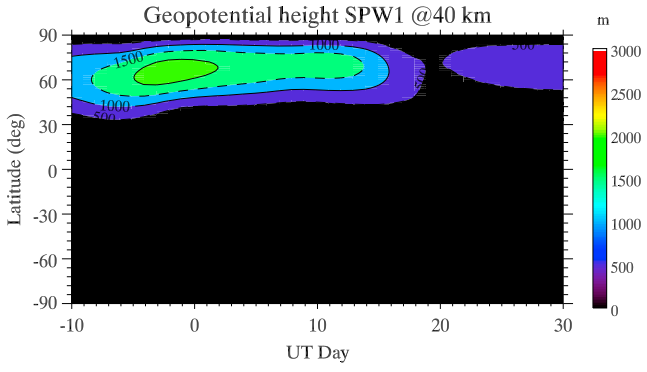

Figure 3. The temporal variations of the zonal wave number 1 stationary planetary wave at ~40 km. Day 1 represents 1 January 2012.

Figure 3 shows the amplitude of the SPW1 in geopotential height, which is obtained from European Centre for Medium-Range Weather Forecasts (ECMWF) data set at ~40 km (2 hPa). It is clear that the activities of the SPW1 are mostly confined to high latitudes of the northern/winter hemisphere with a

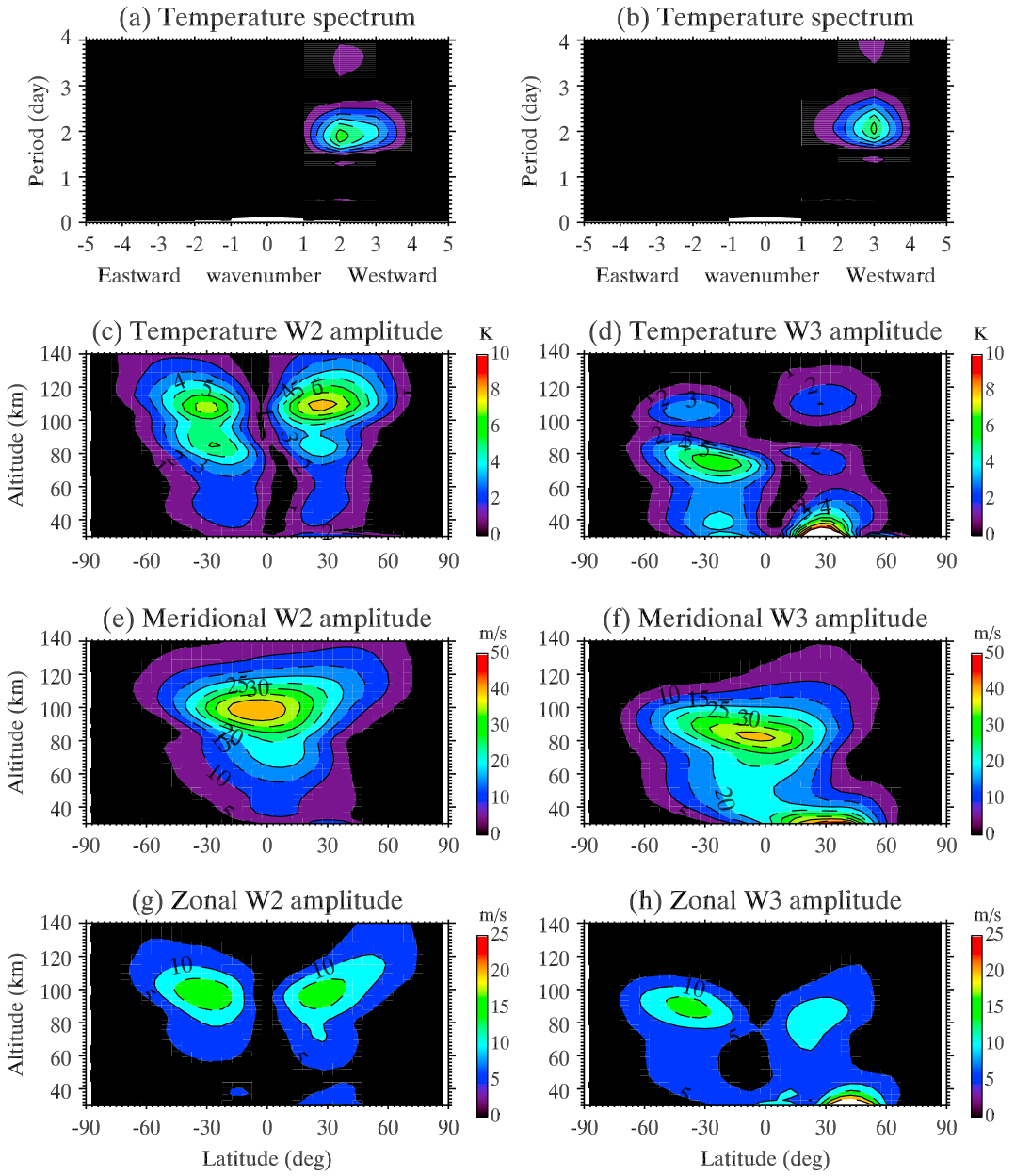

Figure 4. The same as Figure 1 but for TIME-GCM simulations results. The results of (a, c, e, and g) W2 QTDW are obtained with data sets during model days 15–20, and the results of (b, d, f, and h) W3 QTDW are obtained with data sets during model days 25–30.

maximum at ~60°N. The SPW1 reaches the strongest amplitude of ~2500 m at the end of December 2011 and the beginning of January 2012.

Teitelbaum and Vial [1991] proposed that the nonlinear interaction between two waves results in two child waves, whose frequencies and zonal wave numbers are the sum and difference of the two parent waves. And the energy of the child waves come from the parent waves during the nonlinear interaction. For the nonlinear interactions between W3 QTDW and SPW1, the frequencies (f) and zonal wave numbers (s) of the parent waves are as follows: (f, s) = (0.5, 3) and (0, 1). Thus, the child waves are as follows: (f, s) = (0.5, 4) and (0.5, 2). Note here that positive s indicates a westward propagating wave. At the beginning of January 2012 when W2 QTDW maximizes, the amplitude of the W3 QTDW is about one third of its primary peak on 23 January (Figure 2), while the SPW1 is still very strong (larger than 1500 m according to Figure 3). Moreover, the

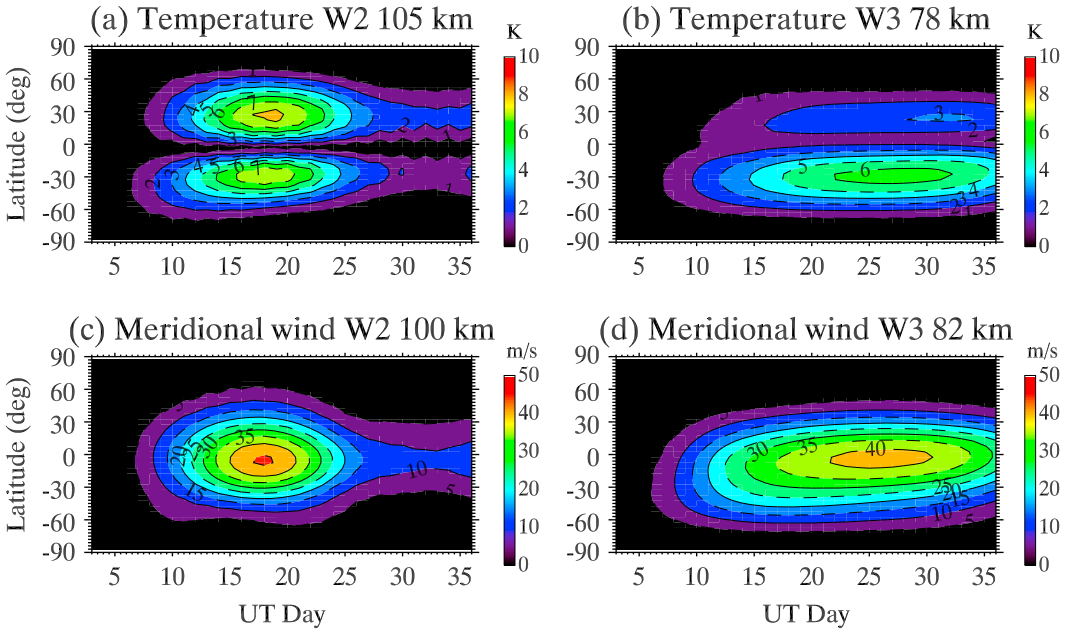

Figure 5. The temporal variations of the W2 QTDW in (a) temperature at ~105 km and (c) meridional wind at ~100 km and of the W3 QTDW in (b) temperature at ~78 km and (d) meridional wind at ~82 km for TIME-GCM simulations.

secondary W2 QTDW peak on around 13 January 2012 coincides with a secondary peak of W3 QTDW. On 23 January when W3 maximizes, the SPW1 amplitude is about 500 m. It is thus seen that the W2 QTDW becomes large when both the W3 component and SPW1 are large, in general agreement with the nonlinear interaction theory.

To further test and verify the nonlinear interactions between the W3 QTDW and SPW1, the TIME-GCM is utilized by specifying both W3 QTDW and SPW1 perturbations at the lower model boundary simultaneously. Note that no W2 QTDW perturbations are forced at the lower boundary. Figure 4a shows the wave number-period spectrum of temperature during model days 15–20 and the dominant component is QTDW with westward wave number 2. The wave number-period spectra of other components, e.g., meridional and zonal winds, display similar wave features as the meridional wind (not shown here). We should emphasize that W3 QTDW and SPW1 are the only planetary waves specified at the lower boundary in this TIME-GCM simulation, and no W2 QTDW signals are detected in the additional TIME-GCM runs with only W3 QTDW without SPW1 perturbations imposed at the lower boundary. Thus, the W2 QTDW signatures in the model simulation are most likely generated by the nonlinear interaction between W3 QTDW and SPW1. Figure 4c shows the latitude-vertical structure of the W2 QTDW in temperature. Like the SABER results in Figure 1c, the simulated W2 QTDW in temperature also peaks at middle latitude with minimum amplitude at the equator. The temperature perturbations show a stronger peak between 100 km and 110 km and a weaker peak between 80 km and 90 km, which also agrees with the SABER temperature observations, especially in the Southern Hemisphere. Figure 4e shows the cross section of the W2 QTDW in TIME-GCM meridional wind for model days 15–20. It maximizes in the equatorial region at ~100 km, which agrees well with the TIDI wind observations. Shown in Figure 4g is the structure of the W2 QTDW in zonal wind, and it peaks at middle latitude with an amplitude about half of the maximum meridional wind amplitude.

Figure 4b shows the wave number-period spectrum of the temperature during model run days 25–30, which is dominated by the QTDW with westward wave number 3. Figure 4d shows the latitude-vertical structure of the W3 QTDW in temperature, and it also peaks at middle latitudes in both hemispheres with the perturbations being stronger in the summer hemisphere. The temperature perturbations show two peaks at ~75 and ~105 km in both hemispheres, but with the peak altitude of 75 km in simulation being slightly higher than the observations. Figures 4f and 4h show the cross section of the W3 QTDW in meridional and zonal winds, respectively, which are obtained with TIME-GCM simulations during model days 25–30. The meridional wind maximizes in the equatorial region at ~100 km, while the zonal wind perturbations peak at

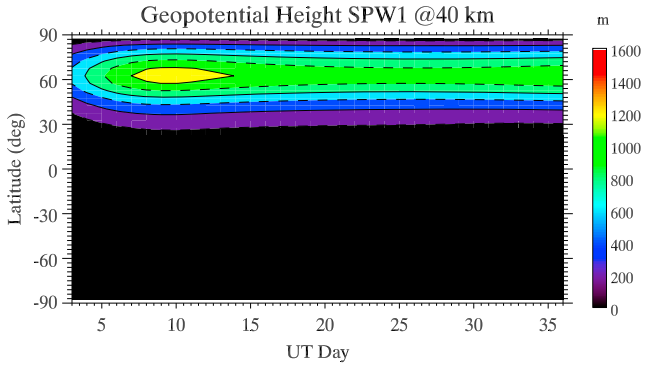

Figure 6. The temporal variations of the SPW1 in geopotential height at ~40 km (2 hPa) for the TIME-GCM simulations.

middle latitudes with amplitude about half of the meridional wind. Generally, both the temperature and horizontal wind structures of W3 QTDW agree with the SABER and TIDI observations.

Figures 5a and 5b show the temporal variations of the W2 and W3 QTDW in TIME-GCM temperature at ~105 and ~78 km, respectively. The temperature perturbations of the W2 QTDW peak between days 15 and 20 with amplitudes of ~7 K in the Southern Hemisphere and ~8 K in the Northern Hemisphere. The W3 QTDW in temperature maximizes during days 25–30 with amplitudes of ~3 K in the Northern Hemisphere and ~6 K in the Southern Hemisphere. Figures 5c and 5d show the temporal variations of the W2 and W3 QTDW in TIME-GCM meridional wind at 100 km and 82 km, respectively. The perturbations of the W2 QTDW in meridional wind also peak between days 15 and 20 with amplitude of ~45 m/s, leading the maximum W3 QTDW amplitude of ~40 m/s between days 25 and 30. Figure 6 shows the amplitudes of the SPW1 in geopotential height at ~40 km for the TIME-GCM simulations. Note that the amplitude of SPW1 decreases from day 10 as the amplitude of W2 QTDW increases, which is also shown in Figure 3 for the observations. There are two possible reasons for the attenuation of SPW1. One, the background zonal wind is decelerated or even reversed by the strong planetary wave at winter high-latitude region, which in return prevents the propagation of the planetary wave itself. Second, the energy of SPW1 is transmitted to the child waves (e.g., W2 QTDW) during the nonlinear interaction [*Teitelbaum and Vial*, 1991].

According to the nonlinear interactions theory, both W2 and W4 QTDW are generated in the nonlinear interaction. However, no significant W4 signatures are detected in either the observations or TIME-GCM simulations. We should note that the phase speed of the W4 is only half as large as W2 QTDW, which means that the W4 is more vulnerable to dissipation and critical layer filtering when propagating upward [*Salby and Callaghan*, 2001]. The W2 QTDW, on the other hand, propagates faster than W4 (and W3) QTDW and can thus propagate and grow more readily. This is a possible reason why W2 QTDW peaks earlier than W3 QTDW in both observations and TIME-GCM simulations.

Figure 7 shows the Eliassen-Palm (EP) flux of W2 during model days 15–20 and its divergence. The zonal mean zonal wind and the potential mean flow instability region are also shown. In our simulation, both the W3 QTDW and SPW1 are forced at the lower model boundary (~10 hPa) in the Northern Hemisphere, which agrees with the planetary wave signals in ECMWF data sets. Thus, it is reasonable to anticipate the nonlinear interaction to occur in the Northern Hemisphere at lower model boundary. However, the EP flux of W2 QTDW and its divergence show two other sources for W2. One source resides between 50 and 80 km at middle and high latitudes in the Southern Hemisphere, which is most likely related to the additional amplification by the summer easterly mean flow instabilities. The other one resides between 50 and 100 km in the Northern Hemisphere, which possibly

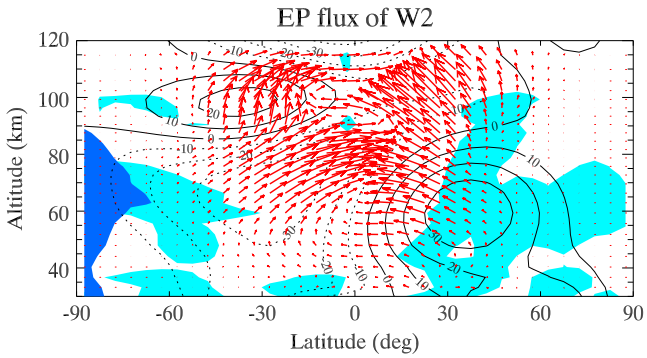

Figure 7. The EP flux (red arrow) of the W2 QTDW during model days 15–20 and its positive divergence regions (light blue shades). The zonal mean zonal wind is overplotted with dotted (westward) and solid (eastward) lines. The potential baroclinic/barotropic instability region is overplotted with blue shades.

results from the auxiliary nonlinear interaction between W3 QTDW and SPW1. The detailed information about the nonlinear coupling between the W3 QTDW and SPW1 during sudden stratospheric warming (SSW) period is beyond the scope of this paper.

4. Summary

A W2 QTDW is identified in both the SABER temperature and TIDI horizontal wind observations in the MLT region at the beginning of January 2012, which coincides with a strong SPW1 episode at high latitude of the northern winter hemisphere. The TIME-GCM is then utilized to simulate the nonlinear interaction between W3 QTDW and SPW1 by specifying W3 QTDW and SPW1 perturbations at the lower model boundary. It is found that the W2 QTDW is generated through the nonlinear interaction, and the simulation results agree well with the temperature and wind observations. This study provides the first strong evidence for the nonlinear interaction between the W3 QTDW and SPW1 from both observations and simulations. The seasonal and interannual variations of the W2 QTDW will be statistically investigated with long-term TIMED observations in the future. It would be interesting to see if the amplification of W2 QTDW always coincides with strong W3 QTDW or SPW1 activities. The amplification of the W2 QTDW and the potential influences of the SSW on QTDW will be studied in detail in a separate paper.

Acknowledgments

This work is carried out at the National Center for Atmosphere Research, with support from the China Scholarship Council. The National Center for Atmospheric Research is sponsored by the National Science Foundation. We would like to acknowledge high-performance computing support from Yellowstone (ark:/85065/d7wd3xhc) provided by NCAR's Computational and Information Systems Laboratory, sponsored by the National Science Foundation. H.L. acknowledges support from NSF grant AGS-1138784. T.L. and X.D.'s work is supported by the National Natural Science Foundation of China grants (41225017, 41127901, 41025016, and 41121003); the Chinese Academy of Sciences Key Research Program KZZD-EW-01; the National Basic Research Program of China grant 2012CB825605; and the Fundamental Research Funds for the Central Universities. The TIDI and SABER data sets are downloaded at http://timed.hao.ucar.edu/tidi/data.html and http://saber.gats-inc.com/, respectively. The ECMWF data set is obtained from http://data-portal.ecmwf.int/data/d/interim_daily/levtype=pl/.

Alan Rodger thanks the reviewers for their assistance in evaluating this paper.

References

Gu, S. Y., T. Li, X. K. Dou, Q. Wu, M. G. Mlynczak, and J. M. Russell (2013), Observations of quasi-two-day wave by TIMED/SABER and TIMED/TIDI, *J. Geophys. Res. Atmos.*, *118*, 1624–1639, doi:10.1002/jgrd.50191.

Killeen, T. L., Q. Wu, S. C. Solomon, D. A. Ortland, W. R. Skinner, R. J. Niciejewski, and D. A. Gell (2006), TIMED Doppler Interferometer: Overview and recent results, *J. Geophys. Res.*, *111*, A10S01, doi:10.1029/2005JA011484.

Limpasuvan, V., and D. L. Wu (2009), Anomalous two-day wave behavior during the 2006 austral summer, *Geophys. Res. Lett.*, *36*, L04807, doi:10.1029/2008GL036387.

Limpasuvan, V., C. B. Leovy, and Y. J. Orsolini (2000), Observed temperature two-day wave and its relatives near the stratopause, *J. Atmos. Sci.*, *57*(11), 1689–1701, doi:10.1175/1520-0469(2000)057<1689:OTTDWA>2.0.CO;2.

Lindzen, R. S. (1981), Turbulence and stress owing to gravity wave and tidal breakdown, *J. Geophys. Res.*, *86*, 9707–9714, doi:10.1029/JC086iC10p09707.

Liu, H.-L., E. R. Talaat, R. G. Roble, R. S. Lieberman, D. M. Riggin, and J.-H. Yee (2004), The 6.5-day wave and its seasonal variability in the middle and upper atmosphere, *J. Geophys. Res.*, *109*, D21112, doi:10.1029/2004JD004795.

Liu, H.-L., W. Wang, A. D. Richmond, and R. G. Roble (2010), Ionospheric variability due to planetary waves and tides for solar minimum conditions, *J. Geophys. Res.*, *115*, A00G01, doi:10.1029/2009JA015188.

Mertens, C. J., et al. (2004), SABER observations of mesospheric temperatures and comparisons with falling sphere measurements taken during the 2002 summer MaCWAVE campaign, *Geophys. Res. Lett.*, *31*, L03105, doi:10.1029/2003GL018605.

Palo, S. E., J. M. Forbes, X. Zhang, J. M. Russell III, and M. G. Mlynczak (2007), An eastward propagating two-day wave: Evidence for nonlinear planetary wave and tidal coupling in the mesosphere and lower thermosphere, *Geophys. Res. Lett.*, *34*, L07807, doi:10.1029/2006GL027728.

Pancheva, D., et al. (2002), Global-scale tidal variability during the PSMOS campaign of June–August 1999: Interaction with planetary waves, *J. Atmos. Sol. Terr. Phys.*, *64*, 1865–1896, doi:10.1016/S1364-6826(02)00199-2.

Pancheva, D., et al. (2004), Variability of the quasi-2-day wave observed in the MLT region during the PSMOS campaign of June–August 1999, *J. Atmos. Sol. Terr. Phys.*, *66*(6–9), 539–565, doi:10.1016/j.jastp.2004.01.008.

Plumb, R. A. (1983), Baroclinic instability of the summer mesosphere: A mechanism for the quasi-two-day wave?, *J. Atmos. Sci.*, *40*(1), 262–270, doi:10.1175/1520-0469(1983)040<0262:BIOTSM>2.0.CO;2.

Riggin, D. M., R. S. Lieberman, R. A. Vincent, A. H. Manson, C. E. Meek, T. Nakamura, T. Tsuda, and Y. I. Portnyagin (2004), The 2-day wave during the boreal summer of 1994, *J. Geophys. Res.*, *109*, D08110, doi:10.1029/2003JD004493.

Roble, R. G., and E. C. Ridley (1994), A thermosphere-ionosphere-mesosphere-electrodynamics general circulation model (time-GCM): Equinox solar cycle minimum simulations (30–500 km), *Geophys. Res. Lett.*, *21*, 417–420, doi:10.1029/93GL03391.

Rojas, M., and W. Norton (2007), Amplification of the 2-day wave from mutual interaction of global Rossby-gravity and local modes in the summer mesosphere, *J. Geophys. Res.*, *112*, D12114, doi:10.1029/2006JD008084.

Salby, M. L. (1981), The 2-day wave in the middle atmosphere: Observations and theory, *J. Geophys. Res.*, *86*, 9654–9660, doi:10.1029/JC086iC10p09654.

Salby, M. L., and P. F. Callaghan (2001), Seasonal amplification of the 2-day wave: Relationship between normal mode and instability, *J. Atmos. Sci.*, *58*(14), 1858–1869, doi:10.1175/1520-0469(2001)058<1858:SAOTDW>2.0.CO;2.

Teitelbaum, H., and F. Vial (1991), On tidal variability induced by nonlinear-interaction with planetary-waves, *J. Geophys. Res.*, *96*, 14,169–14,178, doi:10.1029/91JA01019.

Tunbridge, V. M., D. J. Sandford, and N. J. Mitchell (2011), Zonal wave numbers of the summertime 2 day planetary wave observed in the mesosphere by EOS Aura Microwave Limb Sounder, *J. Geophys. Res.*, *116*, D11103, doi:10.1029/2010JD014567.

Wu, D. L., E. F. Fishbein, W. G. Read, and J. W. Waters (1996), Excitation and evolution of the quasi-2-day wave observed in UARS/MLS temperature measurements, *J. Atmos. Sci.*, *53*(5), 728–738, doi:10.1175/1520-0469(1996)053<0728:EAEOTQ>2.0.CO;2.

Yue, J., H.-L. Liu, and L. C. Chang (2012), Numerical investigation of the quasi 2 day wave in the mesosphere and lower thermosphere, *J. Geophys. Res.*, *117*, D05111, doi:10.1029/2011JD016574.